

THE FUNDAMENTAL PLANE OF THE BROAD-LINE REGION IN ACTIVE GALACTIC NUCLEI

PU DU¹, JIAN-MIN WANG^{1,2,*}, CHEN HU¹, LUIS C. HO^{3,4}, YAN-RONG LI¹ AND JIN-MING BAI⁵

Received 2015 November 21; accepted 2015 December 30

ABSTRACT

Broad emission lines in active galactic nuclei (AGNs) mainly arise from gas photoionized by continuum radiation from an accretion disk around a central black hole. The shape of the broad-line profile, described by $\mathcal{D}_{\text{H}\beta} = \text{FWHM}/\sigma_{\text{H}\beta}$, the ratio of full width at half maximum to the dispersion of broad H β , reflects the dynamics of the broad-line region (BLR) and correlates with the dimensionless accretion rate ($\dot{\mathcal{M}}$) or Eddington ratio ($L_{\text{bol}}/L_{\text{Edd}}$). At the same time, $\dot{\mathcal{M}}$ and $L_{\text{bol}}/L_{\text{Edd}}$ correlate with \mathcal{R}_{Fe} , the ratio of optical Fe II to H β line flux emission. Assembling all AGNs with reverberation mapping measurements of broad H β , both from the literature and from new observations reported here, we find a strong bivariate correlation of the form $\log(\dot{\mathcal{M}}, L_{\text{bol}}/L_{\text{Edd}}) = \alpha + \beta \mathcal{D}_{\text{H}\beta} + \gamma \mathcal{R}_{\text{Fe}}$, where $\alpha = (2.47, 0.31)$, $\beta = -(1.59, 0.82)$ and $\gamma = (1.34, 0.80)$. We refer to this as the fundamental plane of the BLR. We apply the plane to a sample of $z < 0.8$ quasars to demonstrate the prevalence of super-Eddington accreting AGNs are quite common at low redshifts.

Subject headings: black holes: accretion – galaxies: active – galaxies: nuclei

1. INTRODUCTION

Broad emission lines are a hallmark feature of type 1 active galactic nuclei (AGNs) and quasars (Osterbrock & Mathews 1986). As pervasive as they are, many basic properties of the broad-line region (BLR), such as its basic geometry, dynamics, and physical connection to the accretion disk around the supermassive black hole (BH), remain ill-defined. AGN spectra exhibit both tremendous diversity as well as discernable patterns of systematic regularity. Principal component analysis has isolated several dominant relationships among emission-line properties (Boroson & Green 1992; Sulentic et al. 2000). The main varying trend of those properties, which is so-called Eigenvector 1 (EV1), has been demonstrated to be driven by Eddington ratios, $L_{\text{bol}}/L_{\text{Edd}}$, where L_{bol} is the bolometric luminosity and the Eddington luminosity $L_{\text{Edd}} = 1.5 \times 10^{38} (M_{\bullet}/M_{\odot})$ (Boroson & Green 1992; Sulentic et al. 2000; Shen & Ho 2014). As one of the most prominent variables in EV1, the relative strength of broad optical Fe II emission, expressed as

$$\mathcal{R}_{\text{Fe}} = \frac{F_{\text{FeII}}}{F_{\text{H}\beta}}, \quad (1)$$

may correlate with $L_{\text{bol}}/L_{\text{Edd}}$. Sources with high Eddington ratios (accretion rates), for instance so-called narrow-line Seyfert 1 galaxies (Osterbrock & Pogge 1985), emit exceptionally strong Fe II lines compared with the normal ones (Boroson & Green 1992; Hu et al. 2008; Dong et al. 2011). However, the underlying physical mechanism that controls \mathcal{R}_{Fe} remains unclear, as the formation of Fe II is very com-

plex (e.g., Baldwin et al. 2004). It may be influenced by different hydrogen density of BLR gas (Verner et al. 2004), or diverse contribution from microturbulence (Baldwin et al. 2004). In addition, Fe II lags are generally longer by a factor of a few than H β in broad-line Seyfert 1 galaxies (Barth et al. 2013; Chelouche et al. 2014) and roughly equal to H β lags in narrow-line Seyfert 1s (Hu et al. 2015), implying the potential connection of \mathcal{R}_{Fe} with the distribution or structure of line-emitting gas. The $\mathcal{R}_{\text{Fe}} - L_{\text{bol}}/L_{\text{Edd}}$ correlation indicates that Eddington ratios probably regulate all above mentioned properties of BLR. It should be noted that \mathcal{R}_{Fe} also correlates with some other properties like X-ray spectral slopes (e.g., Wang et al. 1996; Laor et al. 1997; Sulentic et al. 2000), but it likely originates from relation of those properties and Eddington ratios (e.g., Wang et al. 2004; Risaliti et al. 2009; Shemmer et al. 2006; Brightman et al. 2013).

The overall breadth of the broad emission lines, notably H β , reflects both the virial velocity and inclination of the BLR (Kollatschny & Zetzl 2011; Shen & Ho 2014). The shape of the line profile may encode more information on the detailed dynamics of the BLR (e.g., Collin et al. 2006; Kollatschny & Zetzl 2011), which itself may depend on fundamental properties such as the accretion or outflow rate. The broad H β lines of NLS1s tend to have more sharply peaked (\sim Lorentzian) profiles compared to type 1 AGNs with more normal Eddington ratios (Véron-Cetty et al. 2001; Zamfir et al. 2010). As a non-parametric description of the line profile, one can define

$$\mathcal{D}_{\text{H}\beta} = \frac{\text{FWHM}}{\sigma_{\text{H}\beta}}, \quad (2)$$

where $\sigma_{\text{H}\beta}$ is the dispersion (second moment) of the H β line. The value of $\mathcal{D}_{\text{H}\beta}$ is 2.35, 3.46, 2.45, 2.83 and 0 for a Gaussian, a rectangular, a triangular, an edge-on rotating ring, and a Lorentzian profiles (for a pure Lorentzian profile $\sigma_{\text{H}\beta} \rightarrow \infty$ and thus $\mathcal{D}_{\text{H}\beta} = 0$), respectively (e.g., Collin et al. 2006). The quantity $\mathcal{D}_{\text{H}\beta}$ correlates loosely with Eddington ratio (Collin et al. 2006) and, as the ratio of the rotational and turbulent components of the line-emitting clouds (Kollatschny & Zetzl 2011), gives a simple, convenient pa-

¹ Key Laboratory for Particle Astrophysics, Institute of High Energy Physics, Chinese Academy of Sciences, 19B Yuquan Road, Beijing 100049, China

² National Astronomical Observatories of China, Chinese Academy of Sciences, 20A Datun Road, Beijing 100020, China

³ Kavli Institute for Astronomy and Astrophysics, Peking University, Beijing 100871, China

⁴ Department of Astronomy, School of Physics, Peking University, Beijing 100871, China

⁵ Yunnan Observatories, Chinese Academy of Sciences, Kunming 650011, China

* Corresponding author, wangjm@mail.ihep.ac.cn

parameter that may be related to the dynamics of the BLR.

While \mathcal{R}_{Fe} and $\mathcal{D}_{\text{H}\beta}$ each correlates separately with Eddington ratio, we demonstrate that both \mathcal{R}_{Fe} and $\mathcal{D}_{\text{H}\beta}$ combined correlate even more tightly with Eddington ratio (and dimensionless accretion rate). This bivariate relation, which we call the “fundamental plane”⁷ of the BLR links two direct observables, plausibly related to the structure and dynamics of the BLR, with the dimensionless accretion rate. Applying the BLR fundamental plane to a large sample of Sloan Digital Sky Survey (SDSS) quasars, we find that a large fraction of quasars at $z < 0.8$ have super-Eddington accretion rates.

2. MEASUREMENTS

2.1. The Reverberation-mapped AGN sample

We select all AGNs with reverberation mapping (RM) data (here only broad $\text{H}\beta$ line), which yield robust BH mass estimates needed for our analysis. All RM AGNs before 2013 are summarized by Bentz et al. (2013). We took all of 41 AGNs from Bentz et al. (2013). Three additional sources (Mrk 1511, NGC 5273, KA1858+4850) were subsequently published. Our project to search for super-Eddington accreting massive black holes (SEAMBHs) has monitored about 25 candidates and successfully measured $\text{H}\beta$ lags ($\tau_{\text{H}\beta}$) in 14 AGNs to date (Du et al. 2015) and other five objects monitored between 2014–2015 (to be submitted). We measure Fe II using the same approach as Hu et al. (2008) and Hu et al. (2015). For reverberation-mapped AGNs without published measurements of Fe II and $\text{H}\beta$ flux, we fit the mean spectra from the monitoring campaigns, using the fitting scheme described in Hu et al. (2015). In short, the spectrum is fitted with several components simultaneously: (1) a power law for continuum, (2) Fe II template from Boroson & Green (1992), (3) host galaxy template if necessary, (4) broad $\text{H}\beta$, (5) broad He II $\lambda 4686$ emission line, and (6) several Gaussians for narrow lines such as [O III] $\lambda\lambda 4959, 5007$. The flux of broad optical Fe II is measured by integration from 4434 Å to 4684 Å. Table 1 lists the 63 RM AGNs we consider, along with the BH mass, 5100 Å luminosity, dimensionless accretion rate, FWHM, $\sigma_{\text{H}\beta}$, \mathcal{R}_{Fe} and data sources.

The sample covers a wide range of accretion rates, $\dot{\mathcal{M}} \approx 10^{-3} - 10^3$, from the regime of a Shakura & Sunyaev (1973) standard disk to a slim disk (Abramowicz et al. 1988). We take \mathcal{R}_{Fe} from the published literature if available; otherwise, we measure it from the averaged spectra following the spectral fitting scheme of Hu et al. (2008, 2015). As the variability of $\text{H}\beta$ is unusually much larger than that of Fe II in sub-Eddington AGNs, the uncertainties of \mathcal{R}_{Fe} are mainly governed by $\text{H}\beta$ variability, which on average is $\sim 20\%$.

We estimate the BH mass as $M_{\bullet} = f_{\text{BLR}} V_{\text{FWHM}}^2 c \tau_{\text{H}\beta} / G$, where f_{BLR} is the virial factor, V_{FWHM} is $\text{H}\beta$ FWHM, and G is the gravitational constant. In practice, the factor f_{BLR} is calibrated against the $M_{\bullet} - \sigma$ relation of inactive galaxies (Onken et al. 2004; Ho & Kim 2014). For consistency with our earlier series of papers, we adopt $f_{\text{BLR}} = 1$.

2.2. Accretion rates and Eddington ratios

We derived accretion rates from the disk model of Shakura & Sunyaev (1973), which has been extensively applied to fit the spectra of quasars and Seyfert

1 galaxies (Czerny & Elvis 1987; Sun & Malkan 1989; Laor & Netzer 1989; Collin et al. 2002; Brockopp et al. 2006; Kishimoto et al. 2008; Davis & Laor 2011; Capellupo et al. 2015). The effective temperature distribution is given by $T_{\text{eff}} = 6.2 \times 10^4 \dot{m}_{\bullet,0.1}^{1/4} m_7^{1/4} R_{14}^{-3/4} \text{K}$, where $\dot{m}_{\bullet,0.1} = \dot{M}_{\bullet} / 0.1 M_{\odot} \text{yr}^{-1}$, \dot{M}_{\bullet} is mass accretion rates, $m_7 = \dot{M}_{\bullet} / 10^7 M_{\odot}$, and $R_{14} = R / 10^{14} \text{cm}$ (Frank et al. 2002). Here the effect of the inner boundary is neglected because the region emitting optical radiation is far from the boundary. Introducing $x = h\nu / kT_{\text{eff}}$, we have the spectral luminosity by integrating over the entire disk,

$$L_{\nu} = 1.58 \times 10^{28} \dot{m}_{\bullet,0.1}^{2/3} m_7^{2/3} \nu_{14}^{1/3} \cos i \int_{x_{\text{in}}}^{\infty} \frac{x^{5/3}}{e^x - 1} dx \text{ erg s}^{-1} \text{ Hz}^{-1}, \quad (3)$$

where i is the disk inclination relative to the observer and $\nu_{14} = \nu / 10^{14} \text{Hz}$. Since long-wavelength photons are radiated from large disk radii, the integral term in Equation (3) can be well approximated by 1.93 for $x_{\text{in}} = 0$ (Davis & Laor 2011). We thus have $\dot{M}_{\bullet} = 0.53 (\ell_{44} / \cos i)^{3/2} m_7^{-1} M_{\odot} \text{yr}^{-1}$, and the dimensionless accretion rate⁸

$$\dot{\mathcal{M}} = 20.1 \left(\frac{\ell_{44}}{\cos i} \right)^{3/2} m_7^{-2}, \quad (4)$$

where ℓ_{44} is the 5100 Å luminosity in units of $10^{44} \text{erg s}^{-1}$. This convenient expression can easily convert luminosity and BH mass into dimensionless accretion rates. In this paper, we take an average value of $\cos i = 0.75$, which corresponds to the opening angle of the dusty torus (e.g., Davis & Laor 2011; Du et al. 2015). The uncertainties of $\dot{\mathcal{M}}$ due to i ($\in [0, 45^\circ]$) are $\Delta \log \dot{\mathcal{M}} = 1.5 \Delta \log \cos i \lesssim 0.15$ from Equation (4), where we took $\Delta \log \cos i \lesssim 0.1$. This uncertainty is significantly smaller than the average error bars of $\log \dot{\mathcal{M}}$ (~ 0.35), and is thus neglected.

The dimensionless accretion rate is related to the more widely used Eddington ratio via $L_{\text{bol}} / L_{\text{Edd}} = \eta \dot{\mathcal{M}}$, where η is the radiative efficiency, and $L_{\text{bol}} \approx 10 L_{5100}$ (Kaspi et al. 2000). The uncertainties of Eddington ratios result from the fact that the bolometric correction depends on both accretion rates and BH mass (Jin et al. 2012). In our following discussion, we will use both $\dot{\mathcal{M}}$ and $L_{\text{bol}} / L_{\text{Edd}}$.

3. FUNDAMENTAL PLANE OF THE BLR

3.1. Correlations

Figure 1a and 1c show the $\mathcal{R}_{\text{Fe}} - (\dot{\mathcal{M}}, L_{\text{bol}} / L_{\text{Edd}})$ plots and yield the following correlations:

$$\mathcal{R}_{\text{Fe}} = \begin{cases} (0.66 \pm 0.04) + (0.30 \pm 0.03) \log \dot{\mathcal{M}}, \\ (1.20 \pm 0.07) + (0.55 \pm 0.06) \log (L_{\text{bol}} / L_{\text{Edd}}). \end{cases} \quad (5)$$

We define the scatter of a correlation as $\Delta_X = \sqrt{\sum_{i=1}^N (X - X_i)^2 / N}$, where N is the number of objects,

⁸ The applicability of Eq. (4) to SEAMBHs can be justified by the self-similar solution of slim disks (Wang et al. 1999; Wang & Zhou 1999). The solution shows that the 5100 Å photons are emitted from $R_{5100} / R_{\text{Sch}} \approx 4.3 \times 10^3 m_7^{-1/2}$, and the photon trapping radius $R_{\text{trap}} / R_{\text{Sch}} \approx 144 \dot{\mathcal{M}}_{100}$, where R_{Sch} is the Schwarzschild radius. Eq. (4) holds provided that $R_{5100} \gtrsim R_{\text{trap}}$, or $\dot{\mathcal{M}} \lesssim 3 \times 10^3 m_7^{-1/2}$. No SEAMBH so far has exceeded this limit.

⁷ Borrowing the terminology from galaxy formation (e.g., Djorgovski & Davis 1987) and accreting BHs (e.g., Merloni et al. 2003)

TABLE 1
THE SAMPLE OF REVERBERATION-MAPPED AGNS

Objects	$\log L_{5100}$ (erg s ⁻¹)	$\log (M_{\bullet}/M_{\odot})$	$\log \mathcal{M}$	FWHM (km s ⁻¹)	σ_{line} (km s ⁻¹)	$\mathcal{D}_{\text{H}\beta}$	\mathcal{R}_{Fe}	Ref.
Mrk 335	43.69 ± 0.06	6.87 ^{+0.10} _{-0.14}	1.17 ^{+0.31} _{-0.30}	2096 ± 170	1470 ± 50	1.43 ± 0.13	0.39	1, 2, 3, 4
	43.76 ± 0.06	7.02 ^{+0.11} _{-0.12}	1.28 ^{+0.30} _{-0.29}	1792 ± 3	1380 ± 6	1.30 ± 0.01	0.77	4, 5, 6 ^a
	43.84 ± 0.06	6.84 ^{+0.18} _{-0.25}	1.39 ^{+0.30} _{-0.29}	1679 ± 2	1371 ± 8	1.23 ± 0.01	0.77	4, 5, 6 ^a
	43.74 ± 0.06	6.92 ^{+0.11} _{-0.14}	1.25 ^{+0.30} _{-0.29}	1724 ± 236	1542 ± 66	1.12 ± 0.16	0.69	4, 7 ^a
	43.76 ± 0.07	6.93^{+0.10}_{-0.11}	1.27^{+0.18}_{-0.17}	1.27 ± 0.05	0.62	4
PG 0026+129	44.97 ± 0.02	8.15 ^{+0.09} _{-0.13}	0.65 ^{+0.28} _{-0.20}	2544 ± 56	1738 ± 100	1.46 ± 0.09	0.33	4, 5, 8 ^a
PG 0052+251	44.81 ± 0.03	8.64 ^{+0.11} _{-0.14}	-0.59 ^{+0.31} _{-0.25}	5008 ± 73	2167 ± 30	2.31 ± 0.05	0.12	4, 5, 8 ^a

NOTE. — All the values of $\log L_{5100}$, $\log(M_{\bullet}/M_{\odot})$ and $\log \mathcal{M}$ are compiled from Du et al. (2015). Values in boldface are the weighted averages of all the measurements for this object.

Ref.: (1) Du et al. 2014; (2) Wang et al. 2014; (3) Hu et al. 2015; (4) Du et al. 2015; (5) Collin et al. 2006; (6) Peterson et al. 1998; (7) Grier et al. 2012; (8) Kaspi et al. 2000.

The superscript *a* for references indicates that \mathcal{R}_{Fe} is measured in this paper; *b* indicates that FWHM and $\sigma_{\text{H}\beta}$ are measured from SDSS spectra (the H β width of SEAMBHs is significantly broadened by the 5'' longslit of our campaign; see details in Ref. 4); *c* means the MCMC BH mass is used (see Section 2.2); *d* means that $\mathcal{D}_{\text{H}\beta}$ is taken from the latest measurements in Kollatschny & Zetzl (2011). NGC 5548 marked with *e* is measured from its mean annual spectra in the AGN watch database; the average value is provided here. We first calculate $\mathcal{D}_{\text{H}\beta}$ for each measurement, and then average. In the main text, we use these averaged numbers for the objects with multiple RM measurements (treated as one point in all figures). For NGC 7469, which was mapped twice Collier et al. (1998) and Peterson et al. (2014), the H β lags are not very different but the H β FWHM is very different; take the values of FWHM measured by Kollatschny & Zetzl (2011). NGC 4051 and PG 1700+518 have very small values of $\mathcal{D}_{\text{H}\beta}$ in Ref. 5, but Kollatschny & Zetzl (2011) provides new measurements, which are used here.

This table is available in its entirety in a machine-readable form in the online journal. A portion is shown here for guidance regarding its form and content.

and *X* represents \mathcal{R}_{Fe} , $\mathcal{D}_{\text{H}\beta}$, \mathcal{M} , or $L_{\text{bol}}/L_{\text{Edd}}$. The Pearson's correlation coefficient (*r*), null-probability (*p*), and scatters are indicated in the plots. By comparing (*r*, *p*, $\Delta_{\mathcal{R}_{\text{Fe}}}$) in panels (a) and (c), we find that the $\mathcal{R}_{\text{Fe}} - \mathcal{M}$ correlation is slightly stronger than that of $\mathcal{R}_{\text{Fe}} - L_{\text{bol}}/L_{\text{Edd}}$. In high- \mathcal{M} AGNs, both H β and continuum variability are significantly smaller than those in sub-Eddington AGNs. On the other hand, Fe II reverberates in a very similarly fashion to H β with respect to the continuum (Hu et al. 2015). Indeed, it can be seen that the scatter of the correlation gets larger with decreasing \mathcal{M} or $L_{\text{bol}}/L_{\text{Edd}}$. The $\mathcal{R}_{\text{Fe}} - (\mathcal{M}, L_{\text{bol}}/L_{\text{Edd}})$ correlations supports the idea that Fe II strength is not governed by metallicity but by the ionizing flux and hydrogen density (Verner et al. 2004).

We plot the $\mathcal{D}_{\text{H}\beta} - (\mathcal{M}, L_{\text{bol}}/L_{\text{Edd}})$ relations in Figure 1b and 1d and find

$$\mathcal{D}_{\text{H}\beta} = \begin{cases} (2.01 \pm 0.05) - (0.39 \pm 0.04) \log \mathcal{M}, \\ (1.28 \pm 0.09) - (0.72 \pm 0.08) \log (L_{\text{bol}}/L_{\text{Edd}}). \end{cases} \quad (6)$$

The above two correlations are similar, but the former is slightly stronger than the latter. Collin et al. (2006) also found a correlation between $\mathcal{D}_{\text{H}\beta}$ and $L_{\text{bol}}/L_{\text{Edd}}$ (see their Figure 6), but their results are much weaker than ours. This is mainly due to the lack of high- \mathcal{M} AGNs in their sample. We would like to emphasize that the $\mathcal{D}_{\text{H}\beta} - (\mathcal{M}, L_{\text{bol}}/L_{\text{Edd}})$ correlations cannot be an artifact of the inclusion of FWHM in \mathcal{M} . For a constant $\sigma_{\text{H}\beta}$ of RM AGNs, the accretion rates span over about 5 dex whereas luminosities span over 4.5; however, the $\mathcal{D}_{\text{H}\beta} - \mathcal{M}$ relation has a scatter of only $\Delta_{\mathcal{D}} = 0.3 - 0.4$. The correlations are intrinsic.

Figure 1 also shows, as background, the SDSS DR5 sample of Hu et al. (2008). The sample comprises 4037 $z \lesssim 0.8$ quasars with criteria of $S/N \geq 10$ and $\text{EW}(\text{Fe II}) \geq 25 \text{ \AA}$ (this excludes Fe II-weak quasars). BH masses assume $f_{\text{BLR}} = 1$

and a standard *R-L* relation⁹. The RM AGNs overlap very well with the SDSS sample, on both the $\mathcal{R}_{\text{Fe}} - (\mathcal{M}, L_{\text{bol}}/L_{\text{Edd}})$ and the $\mathcal{D}_{\text{H}\beta} - (\mathcal{M}, L_{\text{bol}}/L_{\text{Edd}})$ plots. We note that among the mapped AGNs there is a small population ($\lesssim 9\%$; Figure 1a and c) of AGNs with $\mathcal{R}_{\text{Fe}} > 1.4$ of what appear to be super-Eddington sources. Their values of \mathcal{M} are likely underestimated because their black hole masses were estimated using the standard *R-L* relation.

3.2. Fundamental Plane

The $(\mathcal{R}_{\text{Fe}}, \mathcal{D}_{\text{H}\beta}) - (\mathcal{M}, L_{\text{bol}}/L_{\text{Edd}})$ relations reflect connections between the BLR structure and dynamics with BH accretion. We investigate whether these two univariate correlations can be unified into a single bivariate correlation of the form

$$\log(\mathcal{M}, L_{\text{bol}}/L_{\text{Edd}}) = \alpha_k + \beta_k \mathcal{D}_{\text{H}\beta} + \gamma_k \mathcal{R}_{\text{Fe}}, \quad (7)$$

where $(\alpha_k, \beta_k, \gamma_k)$ are coefficients to be determined by data ($k = 1, 2$). We define

$$\chi_k^2 = \frac{1}{N} \sum_{i=1}^N \frac{(\log \mathcal{A}_k^i - \alpha_k - \beta_k \mathcal{D}_{\text{H}\beta}^i - \gamma_k \mathcal{R}_{\text{Fe}}^i)^2}{\sigma_{\mathcal{A}_k}^2 + \beta_k^2 \sigma_{\mathcal{D}_{\text{H}\beta}}^2 + \gamma_k^2 \sigma_{\mathcal{R}_{\text{Fe}}}^2}, \quad (8)$$

where $\mathcal{A}_k = (\mathcal{M}, L_{\text{bol}}/L_{\text{Edd}})$, $\sigma_{\mathcal{A}_k}$, $\sigma_{\mathcal{D}_{\text{H}\beta}}^i$ and $\sigma_{\mathcal{R}_{\text{Fe}}}^i$ are the error bars of $\log \mathcal{A}$, $\mathcal{D}_{\text{H}\beta}$, and \mathcal{R}_{Fe} of the *i*-th object, respectively. Minimizing χ_k^2 , we obtain

$$\alpha_1 = 2.47 \pm 0.34; \quad \beta_1 = -1.59 \pm 0.14; \quad \text{and} \quad \gamma_1 = 1.34 \pm 0.20, \\ \alpha_2 = 0.31 \pm 0.30; \quad \beta_2 = -0.82 \pm 0.11; \quad \text{and} \quad \gamma_2 = 0.80 \pm 0.20.$$

⁹ This is an empirical relation between the BLR size and the continuum. From the recent work of Bentz et al. (2013), it has the form $R_{\text{BLR}} = 33.65 \ell_{44}^{0.53} \text{lt}$. However, Du et al. (2015) found that it only applies to sub-Eddington AGNs; it depends on \mathcal{M} for super-Eddington AGNs. We do not consider the dependence of the *R-L* relation on \mathcal{M} for the SDSS sample in this paper.

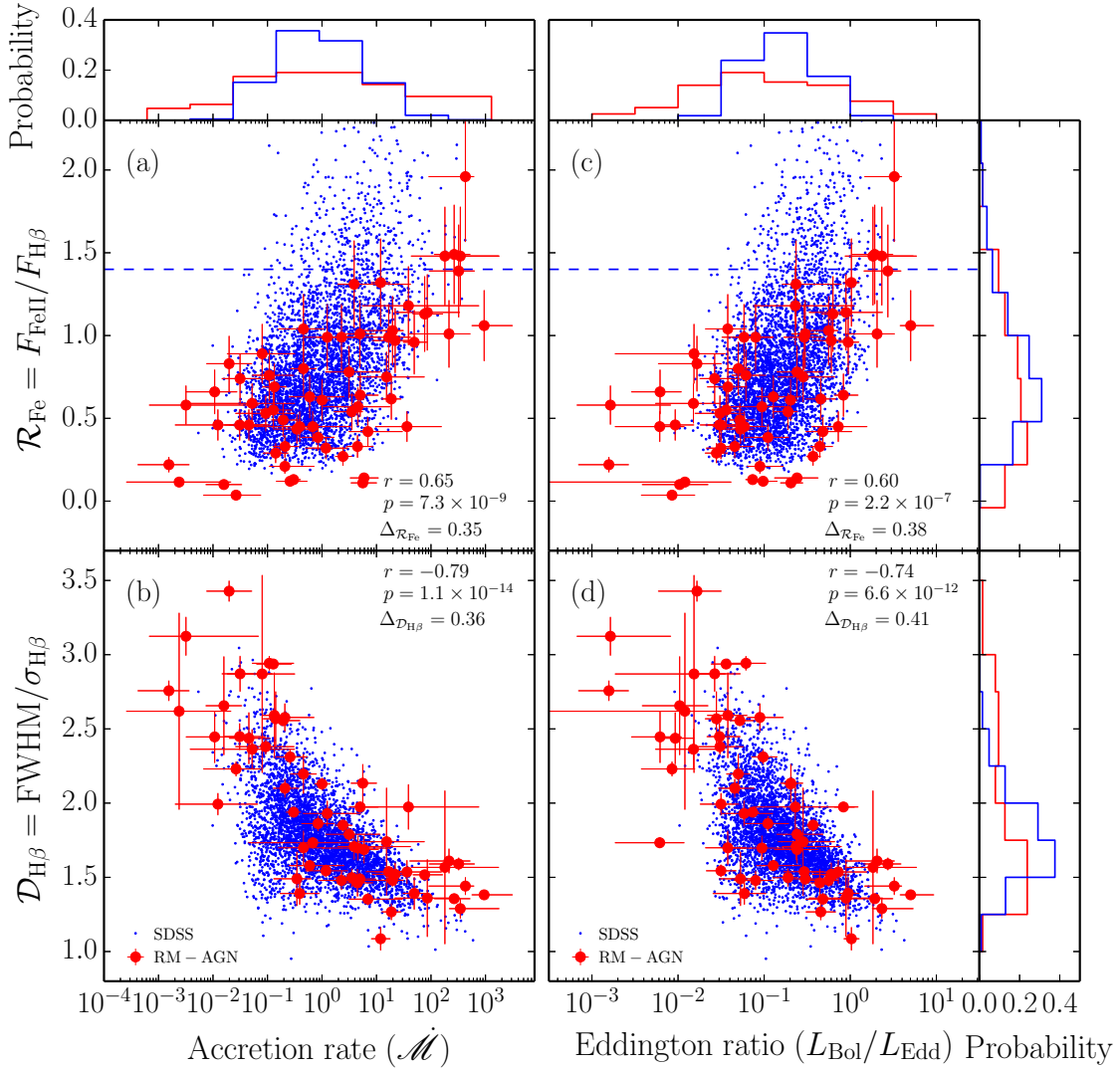


FIG. 1.— Correlations between (a) $\mathcal{R}_{\text{Fe}} - \dot{\mathcal{M}}$ and (b) $\mathcal{D}_{\text{H}\beta} - \dot{\mathcal{M}}$. The Pearson’s coefficient, null-probability, and scatter of the $X - \dot{\mathcal{M}}$ correlation are given by (r, p, Δ_X) . In panel (a), the SDSS quasars overlap with the RM AGNs quite well, except for AGNs with $\mathcal{R}_{\text{Fe}} \gtrsim 1.4$. This could be because these objects are super-Eddington accretors, in which the normal $R - L$ relation (Bentz et al. 2013) overestimates $R_{\text{H}\beta}$ as well as BH mass (Du et al. 2015), and hence $\dot{\mathcal{M}}$ is greatly underestimated (see details in the text). In panel (b), the SDSS sample also overlaps well with the RM AGNs, but the low- $\dot{\mathcal{M}}$ AGNs lie beyond the locus of the SDSS sample. There are some SDSS quasars with extremely high accretion rates, $\dot{\mathcal{M}} \gtrsim 10^2$, suggesting that we should monitor them in the future of SEAMBH project. The histograms indicate the distributions of \mathcal{R}_{Fe} , $\mathcal{D}_{\text{H}\beta}$ and $\dot{\mathcal{M}}$ on a normalized scale. We note that there is no significant correlation between \mathcal{R}_{Fe} and $\mathcal{D}_{\text{H}\beta}$, either in the RM AGN or SDSS sample, indicating that $\mathcal{D}_{\text{H}\beta}$ and \mathcal{R}_{Fe} are independent from each other, although both correlate with $\dot{\mathcal{M}}$. Panels (c) and (d) are the same as (a) and (b), but for Eddington ratios.

The error bars of $(\alpha_k, \beta_k, \gamma_k)$ are derived from bootstrap simulations. The bivariate correlations, plotted in Figure 2, are much stronger than individual corrections of Figure 1 (see the correlation coefficients and null-probability). We call these new correlations as the fundamental plane of the BLR.

The implications of Equation (7) are exciting. From two simple measurements of a single-epoch spectrum of a quasar—strength of Fe II and shape of broad H β —we can deduce the status of its accretion flow. This can be very useful when applied to large samples of quasars to investigate the cosmological growth of BHs. Our method can be usefully applied to quasars with suitable spectroscopy in the rest-frame H β region, for which the strength of Fe II can be measured or constrained.

3.3. Application to SDSS sample

We apply the $\dot{\mathcal{M}}$ -plane (Equation 7) to a sample of 4037 objects Hu et al. (2008), which were selected from the SDSS DR5 sample composed of $N_{\text{tot}} \approx 15,000$ quasars with $z \lesssim 0.8$. We calculate fractions of quasars with $\dot{\mathcal{M}} \geq \dot{\mathcal{M}}_c$, $\delta = N_{\dot{\mathcal{M}}_c} / N_{\text{tot}}$, where $N_{\dot{\mathcal{M}}_c}$ is the number of quasars and $\dot{\mathcal{M}}_c$ is the critical accretion rate in question. For objects with $\dot{\mathcal{M}} \geq 3$, we find $\delta_3 = N_3 / N_{\text{tot}} \approx 0.18$. Similarly, we have $\delta_{10} = N_{10} / N_{\text{tot}} \approx 0.12$ and $\delta_{100} = N_{100} / N_{\text{tot}} \approx 0.02$. These numbers show that super-Eddington accreting AGNs are quite common in the Universe at $z < 0.8$. We should note that these fractions are lower limits, as a result of the selection criteria imposed by Hu et al. Detailed results of the application of our technique to the latest sample of SDSS quasars will be carried out in a separate paper.

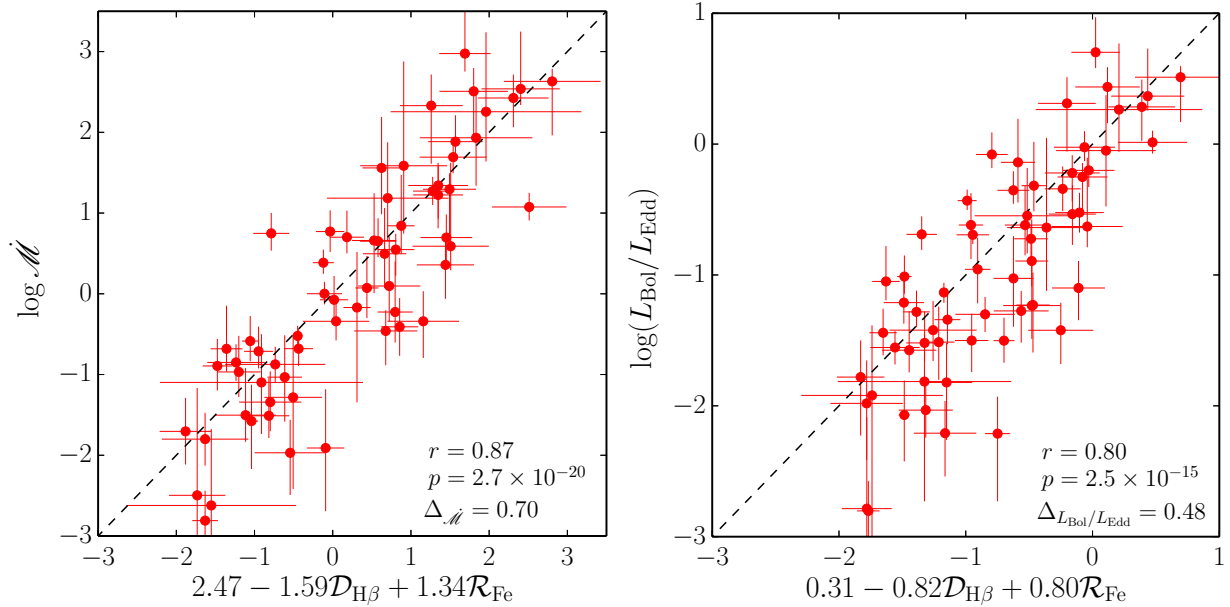


FIG. 2.— The fundamental plane of AGN BLRs, showing a physical connection between accretion disks and BLRs. The dependent variable is (left) \dot{M} and (right) Eddington ratio. The two observables of R_{Fe} and $D_{\text{H}\beta}$ can be readily measured from single-epoch spectra, allowing us to constrain the accretion status of the central engine.

4. CONCLUSIONS

This paper studies correlations among three dimensionless AGN parameters: accretion rate (or Eddington ratio), shape of the broad $\text{H}\beta$ line, and flux ratio of optical Fe II to $\text{H}\beta$. A strong correlation among them is found, which we denote as the fundamental plane of AGN BLRs (Equation 7). The BLR fundamental plane enables us to conveniently explore the accretion status of the AGN central engine using single-epoch spectra, opening up many interesting avenues for exploring AGNs, including their cosmological evolution. A simple ap-

plication of the BLR fundamental plane shows that super-Eddington accreting AGNs are quite common in among low-redshift quasars.

This research is supported by the Strategic Priority Research Program - The Emergence of Cosmological Structures of the Chinese Academy of Sciences, Grant No. XDB09000000, by NSFC grants NSFC-11173023, -11133006, -11373024, -11233003 and -11473002, and a NSFC-CAS joint key grant of U1431228.

REFERENCES

- Abramowicz, M. A., Czerny, B., Lasota, J.-P., & Szuszkiewicz, E. 1988, *ApJ*, 332, 646
- Baldwin, J. A., Ferland, G. J., Korista, K. T., Hamann, F., & LaCluyzé, A. 2004, *ApJ*, 615, 610
- Barth, A. J., Pancoast, A., Bennert, V. N. et al. 2013, *ApJ*, 769, 128
- Bentz, M. C., Denney, K. D., Grier, C. J., et al. 2013, *ApJ*, 767, 149
- Brightman, M., Silverman, J. D., Mainieri, V., et al. 2013, *MNRAS*, 433, 2485
- Brocksopp, C., Starling, R. L. C., Schady, P., et al. 2006, *MNRAS*, 366, 953
- Boroson, T. A., & Green, R. F. 1992, *ApJS*, 80, 109
- Capellupo, D. M., Netzer, H., Lira, P. et al., 2015, *MNRAS*, 446, 3427
- Chelouche, D., Rafter, S. E., Cotlier, G. I. & Barth, A. J. 2014, *ApJ*, 783, L34
- Collier, S. J., Horne, K., Kapsi, S., et al. 1998, *ApJ*, 500, 162
- Collin, S., Boisson, C., Mouchet, M., et al. 2002, *A&A*, 388, 771
- Collin, S., Kawaguchi, T., Peterson, B. M., & Vestergaard, M. 2006, *A&A*, 456, 75
- Czerny, B., & Elvis, M. 1987, *ApJ*, 321, 305
- Davis, S. W. & Laor, A. 2011, *ApJ*, 728, 98
- Djorgovski, S., & Davis, M. 1987, *ApJ*, 313, 59
- Dong, X.-B., Wang, J.-G., Ho, L. C., et al. 2011, *ApJ*, 736, 86
- Du, P., Hu, C., Lu, K.-X., et al. 2014, *ApJ*, 782, 45
- Du, P., Hu, C., Lu, K.-X., et al. 2015, *ApJ*, 806, 22
- Frank, J., King, A. R., & Raine, D. J. 2002, *Accretion Power in Astrophysics: Third Edition* (Cambridge: Cambridge Univ. Press)
- Grier, C. J., Peterson, B. M., Pogge, R. W., et al. 2012, *ApJ*, 755, 60
- Ho, L. C. & Kim, M. 2014, *ApJ*, 789, 17
- Hu, C., Du, P., Lu, K.-X., et al. 2015, *ApJ*, 804, 138
- Hu, C., Wang, J.-M., & Ho, L. C. et al. 2008, *ApJ*, 687, 78
- Jin, C., Ward, M., & Done, C. 2012, *MNRAS*, 425, 907
- Kaspi, S., Smith, P. S., Netzer, H., et al. 2000, *ApJ*, 533, 631
- Kishimoto M., Antonucci R., Blaes O., et al. 2008, *Nature*, 454, 492
- Kollatschny, W., & Zetzl, M. 2011, *Nature*, 470, 366
- Laor, A. & Netzer, H. 1989, *MNRAS*, 238, 897
- Laor, A., Fiore, F., Elvis, M., Wilkes, B. J., & McDowell, J. C. 1997, *ApJ*, 477, 93
- Merloni, A., Heinz, S., & di Matteo, T. 2003, *MNRAS*, 345, 1057
- Onken, C. A., Ferrarese, L., Merritt, D., et al. 2004, *ApJ*, 615, 645
- Osterbrock, D. E., & Mathews, W. G. 1986, *ARA&A*, 24, 171
- Osterbrock, D. E., & Pogge, R. W. 1985, *ApJ*, 297, 166
- Peterson, B. M., Grier, C. J., Horne, K., et al. 2014, *ApJ*, 795, 149
- Peterson, B. M., Wanders, I., Bertram, R., et al. 1998, *ApJ*, 501, 82
- Risaliti, G., Young, M., & Elvis, M. 2009, *ApJL*, 700, L6
- Shakura, N. I., & Sunyaev, R. A. 1973, *A&A*, 24, 337
- Shemmer, O., Brandt, W. N., Netzer, H., Maiolino, R., & Kaspi, S. 2006, *ApJL*, 646, L29
- Shen, Y. & Ho, L. C. 2014, *Nature*, 513, 210
- Sulentic, J. W., Marziani, P., & Dultzin-Hacyan, D. 2000, *ARA&A*, 38, 521
- Sun, W.-H., & Malkan, M. A. 1989, *ApJ*, 346, 68
- Verner, E., Bruhweiler, F., Verner, D., et al. 2004, *ApJ*, 611, 780
- Véron-Cetty, M.-P., Véron, P., & Gonçalves, A. C. 2001, *A&A*, 372, 730
- Wang, J.-M., Watarai, K. & Mineshige, S. 2004, *ApJL*, 607, L107
- Wang, J.-M., Du, P., Hu, C., et al. 2014a, *ApJ*, 793, 108
- Wang, J.-M., Szuszkiewicz, E., Lu, F.-J., & Zhou, Y.-Y. 1999, *ApJ*, 522, 839
- Wang, J.-M., & Zhou, Y.-Y. 1999, *ApJ*, 516, 420
- Wang, T., Brinkmann, W., & Bergeron, J. 1996, *A&A*, 309, 81
- Zamfir, S., Sulentic, J. W., Marziani, P., & Dultzin, D. 2010, *MNRAS*, 403, 1759